High-order lattice Boltzmann models for gas flow for a wide range of Knudsen numbers

Léonard De Izarra, Jean-Louis Rouet, Boujema Izrar

HAL Id: insu-00685403

https://hal-insu.archives-ouvertes.fr/insu-00685403

High order lattice Boltzmann models for gas flow on a wide range of Knudsen number

Léonard de Izarra*

Université d'Orléans, Université François Rabelais - Tours,
CNRS/INSU Institut des Sciences de la Terre d'Orléans - UMR 6113 Campus Géosciences 1A,
rue de la Férollerie 45071 Orléans cedex 2, France and
Institut de Combustion, d'Aérothermique, de Réactivité et d'Environnement (ICARE) -CNRS- UPR3021,
1c avenue de la Recherche Scientifique 45071 Orléans cedex 2, France

Jean–Louis Rouet†

Université d'Orléans, Université François Rabelais - Tours,
CNRS/INSU Institut des Sciences de la Terre d'Orléans - UMR 6113 Campus Géosciences 1A,
rue de la Férollerie 45071 Orléans cedex 2, France

Boujema Izrar‡

Institut de Combustion, d'Aérothermique, de Réactivité et d'Environnement (ICARE) -CNRS- UPR3021,
1c avenue de la Recherche Scientifique 45071 Orléans cedex 2, France
(Dated: September 29, 2011)

The lattice Boltzmann methods (LBM) have successfully been applied to micro-scale flows in hydrodynamic regime, such as flows of liquid in porous media. However, the LBM, in their standard formulation, do not produce correct results beyond the hydrodynamic regime, *i.e.* for slip and transitional ones. Following the work of Shan and He [1] we propose to extend the LBM to those stated, where non-equilibrium effects are obvious and require to include a larger number of distribution function moments.

I. INTRODUCTION

The challenge of modeling low-speed gas flow possessing significant non-equilibrium effects, either due to rarefaction or confinement in small size structures, is well known. Such flows are characterized by a finite Knudsen number and a small Mach number $M_a = U_0/c_0 \leq 0.1$, where U_0 is the characteristic velocity of the flow and c_0 the speed of sound. The Knudsen number $K_n = \lambda/L$, defined as the ratio of the mean free path λ of the particles to the characteristic length L of the flow, characterizes the "distance" from equilibrium. For sufficiently large Knudsen, all assumptions of continuum mechanics collapse. More specifically the Navier-Stokes equations and the no-slip boundary conditions are no longer consistent [2].

Since the Boltzmann equation is valid to describe fluid flows at any Knudsen, *i.e.* from hydrodynamic to collisionless regimes, it is a good candidate to model systems with a large range of size scales, namely, where microscopic/rarefied and macroscopic/hydrodynamic scales are connected. Examples of such systems can be found in some natural porous media, such as coal [3], where the size of pores can extend from nanometer to millimeter, or by MEMS [4], which are micro-metric system flows driven by macroscopic pumps.

The Lattice Boltzmann Method (LBM) has recently become a good counterpoint to conventional CFD methods [5], especially to simulate hydrodynamic fluid flows in complex geometries, such as porous media [6].

Furthermore, this method achieves good results for flows with moderate Knudsen ($K_n \sim 0.1$), characteristic of the slip regime, when using kinetics boundary conditions [2, 7] or maximizing an entropy [8]. It would be interesting, for many applications, to improve these methods again so as to access the transitional regime, *i.e.* a Knudsen number of order one. Such an enhancement should help to account for effects related to rarefaction/confinement in porous media, such as the Klinkenberg effect. This has already been studied with standard LBM [9], but dealing with bounce-back or specular boundary conditions which are known to be inefficient at high-Knudsen number when used on their own.

*leonard.de_izarra@cnrs-orleans.fr
†jean-louis.rouet@univ-orleans.fr
‡Boujema.Izrar@cnrs-orleans.fr

For finite Knudsen number, special attention has been given to capture the Knudsen Layer with different kind of LBM models. To keep the computational efficiency of the method, the velocity set has been chosen in accord with a regular lattice (typically the D2Q9 scheme). Nevertheless in order to catch the slip phenomena, effective relaxation time schemes [10, 11] or multiple relaxation time schemes [12, 13, 14, 15] associated with appropriate boundary conditions have been developed. For the D_2Q_9 LBM scheme, Toschi and Succi [16] suggested to add virtual collisions for beams parallels to boundaries, in order to cure the so called "runaway pathology of lattice Boltzmann". Nevertheless, the authors conclude that the standard LBM does not have a sufficient velocity space isotropy. Nie *et al.* [17] come to the same conclusion. Furthermore, using an important number of beams in the discrete velocity models [18], specifically used to solve flows with high Knudsen number, shows that we need a thinner discretization of the velocity space to access high-Knudsen flows.

From those assessments, we propose to study a family of schemes with a reasonably increasing number of beams and an increasing order of isotropy. This family is built on the systematic procedure of construction described by Shan *et al.* [1, 19] which essentially consists in projecting the distribution function on the basis of Hermite polynomials (as in the approach of Grad [20, 21]), and evaluating the moments of this function using the Gauss-Hermite quadrature. Moreover, the present approach may be viewed as a pragmatic alternative to the development given by Shan *et al.* [19]. The non-regular structure of the velocity space that this quadrature induces requires to interpolate for the transport procedure, as already mentioned by Bardow *et al.* [22]. We use the Maxwell's boundary conditions [2, 7] with total accommodation because of the wall importance in high-Knudsen regimes, where inter-particle collisions are nearly absent.

This family of schemes is demonstrated through the numerical simulations of a force-driven plane Poiseuille flow. Numerical results are compared with existing semi-analytical theories [2] and experimental data for various gaseous components [23], which relate the flow rate of the Poiseuille flow to a function of the Knudsen number.

This paper is organized as follows: section II describes the background theory used to build high order lattice Boltzmann models; section III is devoted to the numerical test briefly aforementioned; finally, section IV presents the conclusions and perspectives that can be drawn from this work.

II. HIGH ORDERS LATTICE BGK EQUATIONS

A. The BGK model

The Boltzmann equation describes the evolution of a single particle distribution function, $f(\boldsymbol{x}, \boldsymbol{v}, t)$, where $\boldsymbol{x}$ is the position and $\boldsymbol{v}$ the velocity of the particle at time t. It reads:

$$\frac{\partial f}{\partial t} + \boldsymbol{v} \cdot \boldsymbol{\nabla}_{\boldsymbol{x}} f + \frac{\boldsymbol{F}}{m} \cdot \boldsymbol{\nabla}_{\boldsymbol{v}} f = \left(\frac{\partial f}{\partial t}\right)_c, \tag{1}$$

where $\boldsymbol{\nabla}_{\boldsymbol{x}}$ and $\boldsymbol{\nabla}_{\boldsymbol{v}}$ are respectively the gradients in configurations and velocity spaces, m the mass of a particle and $\boldsymbol{F}$ an external force. In this model, the collision operator (rhs of Eq. (1)) is taken in its linearized form given by Bhatnagar-Gross-Krook (BGK) collision term [24]:

$$\left(\frac{\partial f}{\partial t}\right)_c = -\frac{f - f^{eq}}{\tau}, \tag{2}$$

where τ is the relaxation time. This single time is related to both the kinematic viscosity ν ($\nu = k_B T \tau / m$) and the thermal diffusivity κ ($\kappa = k_B T \tau / m$) of the fluid. This points out that the BGK operator intrinsically describes a fluid for which the Prandt number $P_r = \nu / \kappa$ is equal to unity. Finally, the local Maxwell-Boltzmann equilibrium distribution f^{eq} reads:

$$f^{eq}(\boldsymbol{x}, \boldsymbol{v}, t) = \rho \left(\frac{m}{2 \pi k_B T}\right)^{D/2} exp\left(-\frac{m (\boldsymbol{v} - \boldsymbol{u})^2}{2 k_B T}\right), \tag{3}$$

where k_B is the Boltzmann constant and D the space dimension. The equilibrium distribution function shares the three first moments with f : the density ρ, the macroscopic velocity $\boldsymbol{u}$ and the temperature T, which are all functions of position $\boldsymbol{x}$ and time t. Because the BGK collision operator conserves the number of particles, the momentum and the total energy, those macroscopic quantities are given by the first three momenta of the distribution function f, *i.e.*:

$$\rho = \int f \, d\boldsymbol{v}, \tag{4}$$

$$\rho \, \boldsymbol{u} = \int \boldsymbol{v} \, f \, d\boldsymbol{v}, \tag{5}$$

$$\rho \, D \frac{k_B T}{m} = \int (\boldsymbol{v} - \boldsymbol{u})^2 \, f \, d\boldsymbol{v} \tag{6}$$

B. Discretization procedure

The Lattice Boltzmann Methods (LBM) consist in going back and forth between a kinetic and a macroscopic description. The temporal evolution of the distribution function f is given by (1) where the collisional operator requires to know the equilibrium distribution function f^{eq}. In turn, f^{eq} requires the first three momenta of the distribution function f. The Boltzmann equation is numerically integrated using a splitting scheme [25]. Firstly, the temporal evolution of the distribution function is achieved by solving the linear transport term in the lhs of Eq. (1) alone. Different TVD schemes have been experimented and three flux limiters have been retained and compared : MinMod and Superbee limiters [26] and Koren limiter [27]. They give very close results apart for very low Knudsen numbers ($\leq 10^{-3}$) where the advantage goes to the Koren limiter.

The second step implements the local collisional term. That requires to know the equilibrium function using the three first momenta of the distribution function. The same kind of scheme has already been used to integrate the Vlasov equation [28]. Nevertheless, in this context, it has been recognized that the velocity discretization of the distribution function should be precise enough, especially to take into account high velocities.

Here, because the equilibrium is a Gaussian and because the computation of the momenta of the distribution function requires integral calculation which can be performed efficiently by a Gauss-Hermite quadrature method, we propose to decompose the distribution function on Hermite polynomials basis. The decomposition of the equilibrium function given by Eq. (3) reads:

$$f^{eq} = \rho \, w^{[\theta_0]}(\boldsymbol{v}) \sum_{n=0}^{\infty} \frac{\boldsymbol{u}^n}{n!} \, \mathcal{H}_n^{[\theta_0]}(\boldsymbol{v}), \tag{7}$$

where $w^{[\theta_0]}(\boldsymbol{v}) = 1/\sqrt{2\pi\theta_0} \exp\left(-\boldsymbol{v}^2/2\theta_0\right)$ is the weight function for the Hermite polynomials $\mathcal{H}_n^{[\theta_0]}$, $c_0 = \sqrt{\theta_0} = \sqrt{k_B \, T_0/m}$ the thermal velocity related to an arbitrary temperature θ_0 and $\mathcal{H}_n^{[\theta_0]}$ the n-th Hermite polynomial generalized to the same temperature θ_0 (cf. A). That temperature, although arbitrary, will actually be close to the temperature θ of the system. The summation (7) implies an infinite number of terms. From a practical point of view, the summation is performed up to a given order N. So a truncated equilibrium distribution function $\tilde{f}^{eq}(\boldsymbol{x}, \boldsymbol{v}, t)$ is thus introduced:

$$\tilde{f}^{eq}(\boldsymbol{x}, \boldsymbol{v}, t) = w^{[\theta_0]}(\boldsymbol{v}) \sum_{n=0}^{N} \frac{a_n(\boldsymbol{x}, t)}{n!} \, \mathcal{H}_n^{[\theta_0]}(\boldsymbol{v}), \tag{8}$$

where the coefficients $a_n(x, t)$ are the moments of $\tilde{f}^{eq}$. Again the distribution function f is given by a decomposition on Hermite polynomials basis up to an order q which is not necessarily equal to N:

$$\tilde{f}(\boldsymbol{x}, \boldsymbol{v}, t) = w^{[\theta_0]}(\boldsymbol{v}) \sum_{n=0}^{q} \frac{b_n(\boldsymbol{x}, t)}{n!} \, \mathcal{H}_n^{[\theta_0]}(\boldsymbol{v}), \tag{9}$$

where the $b_n(\boldsymbol{x}, t)$ are computed using the orthogonality relation:

$$b_n(\boldsymbol{x}, t) = \theta_0^n \int_{-\infty}^{\infty} \tilde{f}(\boldsymbol{x}, \boldsymbol{v}, t) \, \mathcal{H}_n^{[\theta_0]}(\boldsymbol{v}) \, d\boldsymbol{v} \tag{10}$$

Because the collision operator conserves the first three moments of f, a_0, a_1 and a_2 are respectively equal to b_0, b_1 and b_2. The higher moments of $\tilde{f}^{eq}$ are combinations of these first three moments. It is natural to compute the integral (10) with a Gauss-Hermite quadrature:

$$
\begin{aligned}
b_m &= \theta_0^m \int_{-\infty}^{\infty} w^{[\theta_0]}(\boldsymbol{v}) \frac{\tilde{f} \, \mathcal{H}_m^{[\theta_0]}(\boldsymbol{v})}{w^{[\theta_0]}(\boldsymbol{v})} \, d\boldsymbol{v} \\
&= \theta_0^m \sum_{i=1}^{q} f_i \, \mathcal{H}_m^{[\theta_0]}(\boldsymbol{v_i}),
\end{aligned}
\tag{11}
$$

with

$$
f_i = \omega_i \, \frac{\tilde{f}(\boldsymbol{x}, \boldsymbol{v_i}, t)}{w^{[\theta_0]}(\boldsymbol{v_i})}
\tag{12}
$$

The velocities $\boldsymbol{v}_i$ are the roots of the Hermite polynomial of order q and the ω_i are their associated weights:

$$
\{\omega_i = q! \left[q \, \mathcal{H}_{q-1}^{[\theta_0]}(v_i) \right]^{-2} : i = 1, \ldots, q\},
\tag{13}
$$

where v_i is the i-th root $\mathcal{H}_q^{[\theta_0]}$.

The summation is exact if the order of the polynomial $\tilde{f} \, \mathcal{H}_m^{[\theta_0]}(\boldsymbol{v})/w^{[\theta_0]}(\boldsymbol{v})$ is less than $2q$. It will then be possible to evaluate the distribution function $\tilde{f}$ up to order q. However, the numerical scheme only needs to construct the equilibrium distribution function $\tilde{f}^{eq}$ explicitly, hence to compute the first three moments of the distribution function. It is consistent with equation (9) to take a Gauss summation up to q. Relation (11) is indeed exact as soon as the order of $\tilde{f}$ is less or equal to q. It will be the case because $\tilde{f}/w_0^{[\theta_0]}(\boldsymbol{v})$ is a polynomial of order q, and $\mathcal{H}_m^{[\theta_0]}$ is a polynomial of order m (m going from 0 to q).

In dimension 1, the discretization of the velocity space is provided by the Gauss-Hermite quadrature. The q velocity values are given by the q roots of the generalized Hermite polynomial $\mathcal{H}_q^{[\theta_0]}(\boldsymbol{v_i})$ (*cf.* A). In higher dimension D, the discretization of the velocity space is obtained by the tensor products of D copies of the 1-dimensional velocity system and the weights are computed as the product of the corresponding 1-dimensional weights. Consequently, the number of velocity beams is q^D. Labeling the distribution function with an index associated to the q^D beams, the three moments read:

$$
\rho = \sum_{i=1}^{q^D} f_i
\tag{14}
$$

$$
\rho \, \boldsymbol{u} = \sum_{i=1}^{q^D} \boldsymbol{v_i} \, f_i
\tag{15}
$$

$$
D \, \rho \, \theta + \rho \, \boldsymbol{u}^2 = \sum_{i=1}^{q^D} \boldsymbol{v_i}^2 \, f_i
\tag{16}
$$

Those three moments allow us to compute a distribution function $f_i^{eq} = \omega_i \, \dfrac{\tilde{f}^{eq}(\boldsymbol{x}, \boldsymbol{v_i}, t)}{w^{[\theta_0]}(\boldsymbol{v_i})}$. For example, the truncation of equation (8) to $N = 2$ provides:

$$
\begin{aligned}
f_i^{eq} &= \omega_i \left(a_0(\boldsymbol{x}, t) \, \mathcal{H}_0^{[\theta_0]}(\boldsymbol{v_i}) + a_1(\boldsymbol{x}, t) \, \mathcal{H}_1^{[\theta_0]}(\boldsymbol{v_i}) + \frac{1}{2} \, a_2(\boldsymbol{x}, t) \, \mathcal{H}_2^{[\theta_0]}(\boldsymbol{v_i}) \right) \\
&= \omega_i \left(\rho + \rho \, \frac{\boldsymbol{u} \cdot \boldsymbol{v_i}}{\theta_0} + \rho \, \frac{(\boldsymbol{u} \cdot \boldsymbol{v_i})^2}{2 \, \theta_0^2} + \rho \, \frac{(\theta - \theta_0)}{2 \, \theta_0} \left(\frac{\boldsymbol{v_i}^2}{\theta_0} - D \right) - \rho \, \frac{\boldsymbol{u}^2}{2 \, \theta_0} \right)
\end{aligned}
\tag{17}
$$

The first three moments of this distribution function are indeed given by a_0, a_1 and a_2. Nevertheless we can show that the positivity of this truncated distribution function is no longer guaranteed. A more complete presentation of this method is given by Shan *et al.* [19]. Here we restrict our study to 2D problems with schemes obtained by 1D composition. So, a scheme called here $\mathcal{H}_q$ (model with q beams per direction) correspond to the quadrature $E_{2,2q-1}^{q^2}$ in [19].

III. NUMERICAL RESULTS

As a benchmark for this method, a transitional-Knudsen-number Poiseuille flows is under study [16]. A force-driven Poiseuille flow was simulated for a large range of Knudsen numbers using schemes based on $\{\mathcal{H}_q : q = 3, \ldots, 8\}$ and with a second order equilibrium distribution function ($N = 2$). These simulations are set-up as follows. We apply Maxwell's boundary conditions in the cross-channel direction (y) and a periodic boundary condition in the channel direction (x). In the cross-stream direction $L = 100$ grid points are employed, and only four grid points are used in the periodic (stream) direction. The Knudsen number is defined as $K_n = \sqrt{\frac{5}{2}} \frac{\nu}{L c_0}$, where ν is the kinematic viscosity and c_0 the speed of sound. Hence, simulations are parametrized using the relation between the kinematic viscosity and the discrete relaxation time $\tau = \nu/c_0^2 - \delta t/2$, with $\delta t = 1$ in dimensionless formulation. The flow is driven by an external force $F = 8 \nu U_0/L^2$ pointing in the positive-x direction, where U_0 is the maximum velocity of the stream in the hydrodynamic limit (*i.e.* for $K_n \to 0$). U_0 is chosen so that every simulation has the same Mach's number: $M_a = U_0/c_0 = 10^{-4}$. Finally, the density, the velocity and temperature are respectively initialized to 1, 0 and θ_0 all over the domain.

For different values of the Knudsen number ($0.001 < K_n < 10$), the mass flow rates across the duct $Q = \sum_{y=0}^{L} \rho(y) u_x(y)$ are calculated when the steady state regime is reached. Figure 1 shows, for each scheme, this mass flow rate normalized to $Q_0 = 6 \nu U_0/c_0$ as a function of K_n. We also give also some experimental values [23] and the low-Knudsen asymptotic value [2] for comparison:

$$\frac{Q}{Q_0} = \frac{1}{6 K_n} + C_1 + 2C_2 K_n. \tag{18}$$

In this expression, the term $1/6 K_n$ (also plotted) is associated to the Navier-Stokes solution without slippage while the other terms involving C_1 and C_2 take into account first and second-order slip boundary condition respectively. Different values could be found in the literature (see Tang *et al.* [9]). Nevertheless C_1 is usually close to 1, while C_2 lives in a wide range of values including negative ones. Here we will take $C_1 = 1$ and $C_2 = .13$ (see hereafter for the choice of C_2).

Figure 1 points out the following observations. Firstly, in the hydrodynamic regime (*i.e.* for $K_n \lesssim 0.01$), all models agree with the theoretical curve given by the Navier-Stokes equations. Even the simplest model $\mathcal{H}_3$, the well known D_2Q_9 which only deals with 3 beams per direction, gives good results. When K_n is increased, the numerical results deviates from the hydrodynamic asymptote as expected, but all models agree with each other almost up to $K_n = 0.1$, value for which discrepancies between them appear. Hence, all these schemes produce good results up to the slip regime, commonly defined in the range $0.01 < K_n < 0.1$.

Beyond the slip regime, *i.e.* in the transitional regime, the flow-rate curves separate, alternating relatively to the experimental curve – our only reference, as no theoretical solution exists in this interval –. This convergence is noticeable because systems with even-order quadrature underestimate the flow-rate, while the odd-order ones overestimate it. However, increasing the order of quadrature improves the result in any case. Physically, the difference between odd and even schemes must be related to the fact that the 0-velocity stream appears in the former but not in the latter. As the 0-velocity particles do not move, they do not collide with boundaries either. They are only sensitive to particle-particle collisions. Unfortunately the influence of this process decreases with increasing Knudsen number and finally, these particles remain in their initial state over a very long time. Although the odd-schemes induce larger errors on the flow-rates, they have the advantage of depicting at least qualitatively a minimum for $Kn \sim 1$. Indeed experimental data reported figure 1 show this minimum which is not an artifact and corresponds exactly to the Knudsen paradox behavior.

The alternation suggests the idea of trying to accelerate the convergence of these schemes by combining two different behavior patterns. The natural choice for these schemes is to take two successive orders. We can therefore hope to compensate the overestimation of the flow-rate of the odd-scheme by the underestimation of the lower or higher even-order, while maintaining the extrema of the curve. These composite schemes are noted $\mathcal{H}_{q|q+1}$ and are simply built by superposition of the $\mathcal{H}_q$ and $\mathcal{H}_{q+1}$ velocity spaces and by dividing the weights of each ones by 2, so the sum of the weights of the new scheme is again equal to unity. More precisely, the new set of velocities of the composite schemes
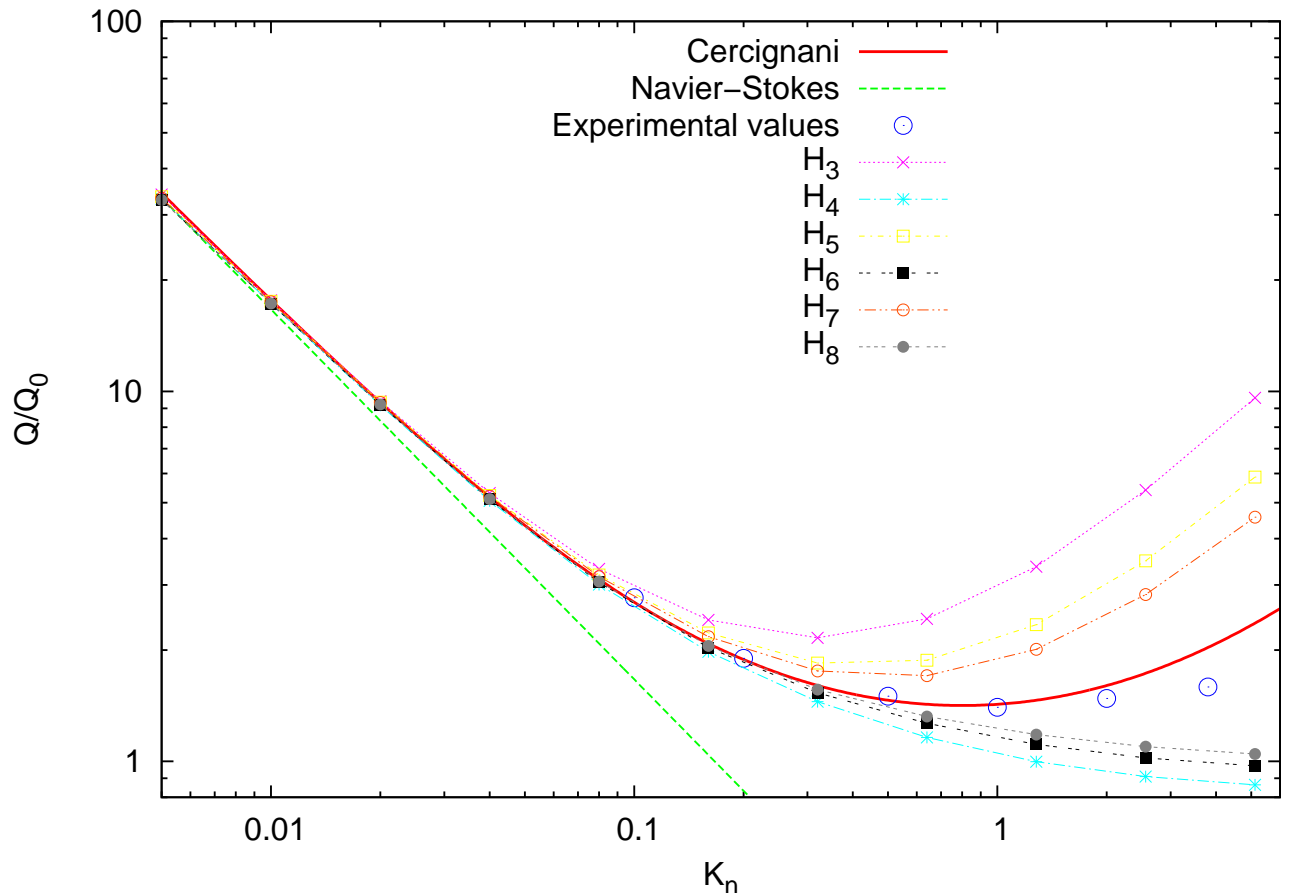
FIG. 1: Q/Q_0 obtained with $\{\mathcal{H}_q : q = 3, \ldots, 8\}$ (symbols), analytical curve (dashed line) and experimental data (stars).

$\mathcal{H}_{q|q+1}$ is the addition of the q^D velocities of $\mathcal{H}_q$ and the $(q+1)^D$ velocities of $\mathcal{H}_{q+1}$ (where D is the spatial dimension). So the transport step of the distribution function is performed for this new set of velocities *i.e.* on $q^D + (q+1)^D$ beams. The equilibrium distribution function is still given by equation (17) but the moments are now computed by summation over the $q^D + (q+1)^D$ f_i's. Here, the weight of a given beam is the same as for the scheme from which it comes, but divided by two. So the sum of the weights over all the beams remains equal to one. As before, the velocities are normalized to the highest one.

On figure 2 are plotted results for the same problem, but obtained with $\{\mathcal{H}_{3|4}, \mathcal{H}_{4|5}, \mathcal{H}_{5|6}, \mathcal{H}_{6|7}\}$ composites schemes described in the previous paragraph. Results of schemes based on $\{\mathcal{H}_q : q = 7, 8\}$ are also plotted for comparison. In terms of computational cost, the $\mathcal{H}_{3|4}$ must be compared with $\mathcal{H}_5$ as they both have 25 beams. $\mathcal{H}_{4|5}$ and $\mathcal{H}_7$ can also be compared as they have respectively 41 and 49 beams. So the combination of two successive order quadratures considerably increases the speed of convergence of the family. Notably, the scheme based on the $\mathcal{H}_{4|5}$ produces very good results up to $K_n = 1$, with a computational cost of the order of standard high-orders lattice Boltzmann models. Finally, the worst behavior of $\mathcal{H}_{5|6}$ compared to $\mathcal{H}_{4|5}$, may be linked to the fact that the relative weight of the 0-velocity stream is more important in the former than in the latter. This suggests to prefer even|odd combination or to give a weight higher then $1/2$ to even models.

To have a better insight into the results, the velocity profiles are given figure 3 for $\mathcal{H}_{4/5}$ and different values of the Knudsen number. The theoretical profiles obtained from an hydrodynamic analysis including a velocity slip is also plotted. Its expression reads :

$$v(x) = 4U_0 \left(\frac{x}{H}(1 - \frac{x}{H}) + C_1 K_n + 2C_2 K_n^2 \right) \tag{19}$$

As expected, the agreement is good for low Knudsen numbers while the numerical profile is flatter than the theoretical one for highest Knudsen values. The slip velocities are given on figure 4 for all models including composite
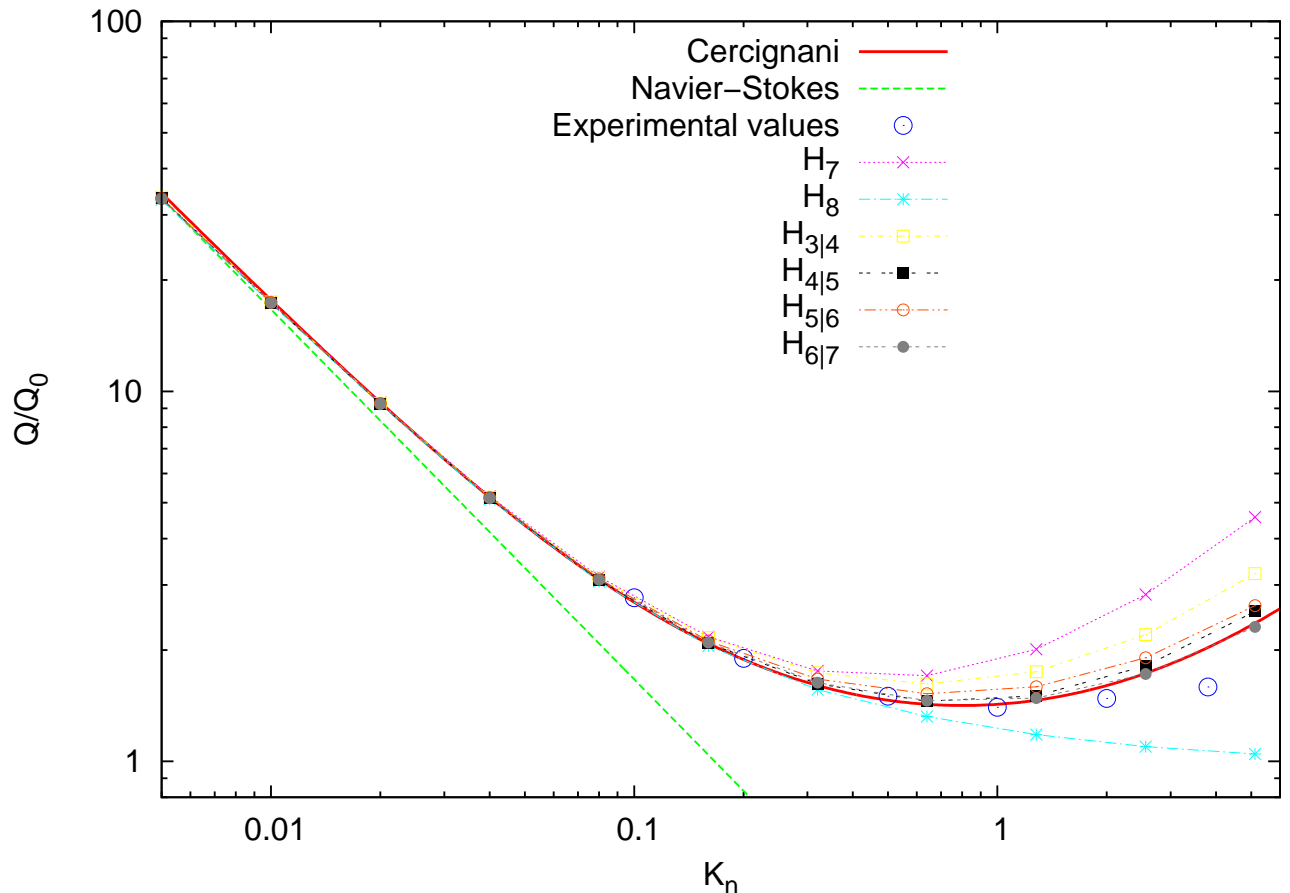
FIG. 2: Flow rate computed with $\{\mathcal{H}_q : q = 7, 8\}$ and $\{\mathcal{H}_{3|4}, \mathcal{H}_{4|5}, \mathcal{H}_{5|6}, \mathcal{H}_{6|7}\}$ (symbols). Experimental data (stars).

ones. The theoretical velocity slip $U_s = v(x = 0)$ obtained with the second order approximation in K_n is given for comparison.

As for equation (18), $C_1 = 1$ and $C_2 = .13$. The value of C_2 has been chosen such that equation (19) fits the slip velocity points of $\mathcal{H}_{4|5}$. As for the flow curve, the same general picture can be drawn : all the models agree in the hydrodynamic limit, while the slip velocity is higher for odd models than for even models. As q increases, the slip velocities of even and odd models converge toward a single curve. This curve is close to the one obtained for the composite models which do not exhibit huge differences.

The computational time needed for the simulations given here is depicted figure 5. For both families of schemes the CPU time scales as the total number of beams to the power 1.32. For the same number of beams, composite schemes are slightly faster than simple ones. More precisely, the numerical effort for a $\mathcal{H}_{q|q+1}$ is approximatively the same as for $\mathcal{H}_{q'}$, with $q' = int([q^D + (q+1)^D]^{1/D})$, where the function $int(x)$ maps x to the closest integer (Fig. 5).

IV. CONCLUSION

We have presented a high order lattice Boltzmann model based on the projection of the distribution function on the Hermite's basis. The schemes obtained with that procedure have been tested on a Poiseuille flow for a wide range of Knudsen numbers, ie from the hydrodynamic regime to the rarefied one. All those schemes agree with the theoretical values for small Knudsen numbers. Two successive order schemes show an alternating convergence toward experimental data. However, that convergence seems to be slow. Mixed scheme have been proposed in order to improve it. Qualitatively the good agreement obtained for $\mathcal{H}_{q+1}$ models coupled to the $\mathcal{H}_q$ ones can be attributed to a finer discretization of the velocity space. For the former, the beams belong to a range around the thermal velocity, while the latter takes into account higher velocities where the probability distribution function is not very
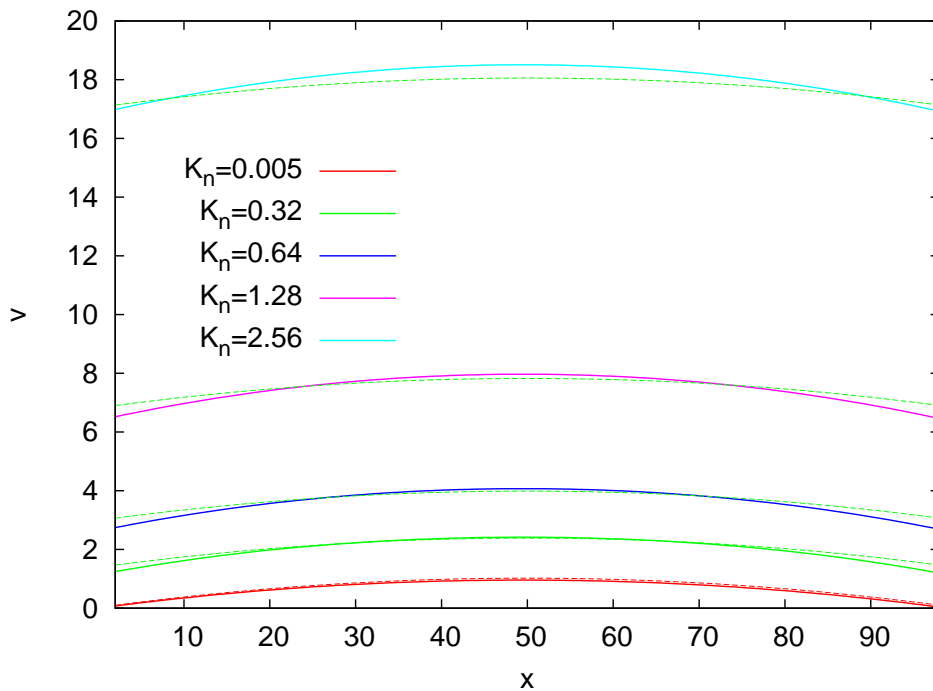
FIG. 3: Velocity profiles for $\mathcal{H}_{4|5}$ and K_n=.005, 0.32, 0.64, 1.28 and 2.56. Numerical results are continuous lines. As expected, theoretical curves (dashed lines) are valid for small Knudsen number.
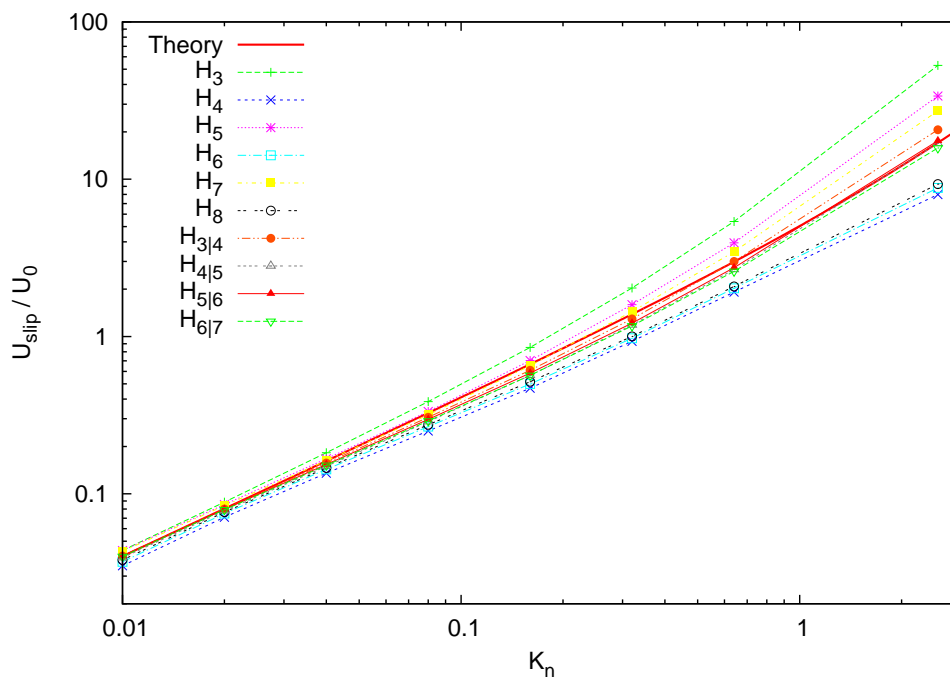

FIG. 4: Slip velocities for $\mathcal{H}_q$ (symbols) and theoretical curve (continuous line).

significant. Among that family the combination of type $\mathcal{H}_{2q+1|2q}$ should be preferred since the 0-velocity stream is weakly weighted.

In our approach, we used a better velocity space discretization than in the usual LBM scheme. In addition, to be
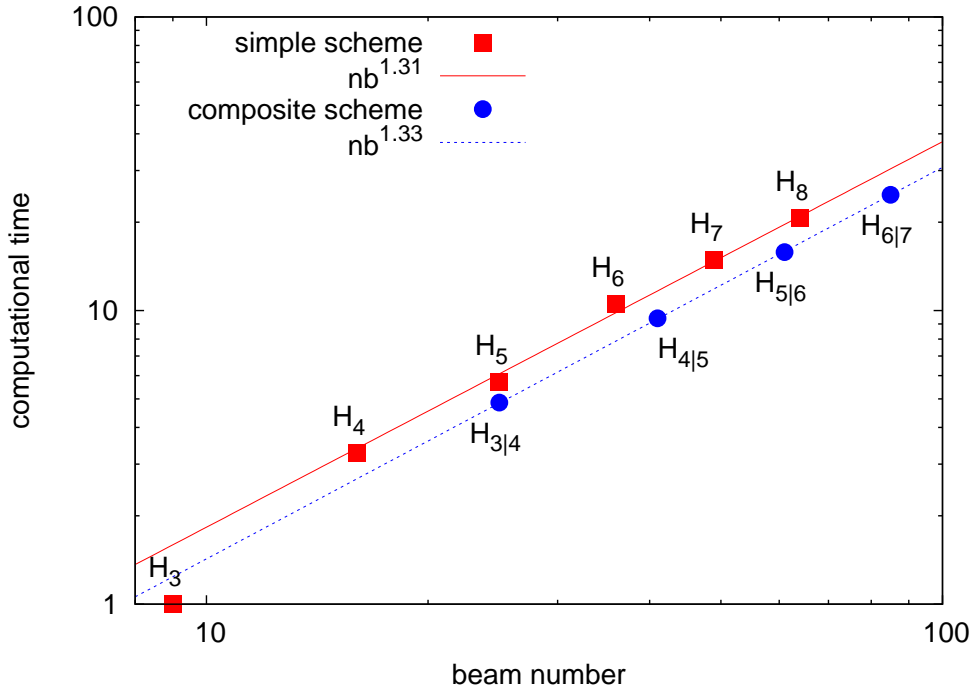
FIG. 5: Normalized CPU time for the different models with $K_n = 0.032$.

able to use Gauss Hermite quadrature to compute the exact the moments of the distribution function, the velocities are the roots of an Hermite polynomial. The irrationality of these roots demands the use of a more sophisticated propagation step than for a standard lattice method. To that respect, the computational effort is more important. Nevertheless, all the schemes imply the usual relaxation time related directly to the Knudsen number. So there is no need to introduce an effective scheme-dependent relaxation time nor to use a multiple relaxation time scheme. In the former case it appears that it is still a challenge to find a general wall function.

The scheme order is related to the truncation q of the Hermite development of the distribution function (see Eq. (7)) which is higher than the truncation N of the equilibrium distribution function toward which the former relaxes. Here, we have taken $N = 2$, while q runs from 2 to 8. Although it is not explicitly computed, it is important to have a good description of the distribution function, especially for high Knudsen values for which it remains out of equilibrium over long times. It has been numerically verified that, at least for the benchmark presented here, increasing the order N only has minor influence.

Acknowledgments

APPENDIX A: HERMITE POLYNOMIALS

1. Appendix I

Generalized Hermite polynomials with temperature $\theta_0 = c_0^2$.

$$\mathcal{H}_0^{[c_0^2]}(x) = 1 \qquad\qquad \mathcal{H}_3^{[c_0^2]}(x) = \frac{x^3}{c_0^6} - \frac{3\,x}{c_0^4}$$

$$\mathcal{H}_1^{[c_0^2]}(x) = \frac{x}{c_0^2} \qquad\qquad \mathcal{H}_4^{[c_0^2]}(x) = \frac{x^4}{c_0^8} - \frac{6\,x^2}{c_0^6} + \frac{3}{c_0^4}$$

$$\mathcal{H}_2^{[c_0^2]}(x) = \frac{x^2}{c_0^4} - \frac{1}{c_0^2} \qquad\qquad \mathcal{H}_5^{[c_0^2]}(x) = \frac{x^5}{c_0^{10}} - \frac{10\,x^3}{c_0^8} + \frac{15\,x}{c_0^6}$$

2. Appendix II

Generalized Hermite polynomials with temperature $\theta_0 = c_0^2$ in dimension higher than one.

$$\boldsymbol{\mathcal{H}}_0^{[c_0^2]}(\boldsymbol{x}) = 1 \qquad\qquad \boldsymbol{\mathcal{H}}_{1\,\alpha}^{[c_0^2]}(\boldsymbol{x}) = \frac{x_\alpha}{c_0^2}$$

$$\boldsymbol{\mathcal{H}}_{2\,\alpha\,\beta}^{[c_0^2]}(\boldsymbol{x}) = \frac{x_\alpha\,x_\beta}{c_0^4} - \frac{\delta_{\alpha\,\beta}}{c_0^2} \qquad\qquad \boldsymbol{\mathcal{H}}_{3\,\alpha\,\beta\,\gamma}^{[c_0^2]}(\boldsymbol{x}) = \frac{x_\alpha\,x_\beta\,x_\gamma}{c_0^6} - \frac{x_\alpha\,\delta_{\beta\,\gamma} + x_\beta\,\delta_{\alpha\,\gamma} + x_\gamma\,\delta_{\alpha\,\beta}}{c_0^4}$$

$\boldsymbol{\mathcal{H}}_n^{[c_0^2]}$ is a tensor of order n.

[1] X. Shan and X. He, Phys. Rev. Lett. **80**, 65 (1998).
[2] C. Cercignani, *The Boltzmann Equation and Its Applications*, vol. 67 of *Applied Mathematical Sciences* (Springer, Berlin, Germany; New York, U.S.A., 1994).
[3] C. F. Rodrigues and M. J. L. de Sousa, International Journal of Coal Geology **48**, 245 (2002), ISSN 0166-5162.
[4] X. Nie, G. D. Doolen, and S. Chen, Journal of Statistical Physics **107**, 279 (2002), ISSN 0022-4715, 10.1023/A:1014523007427.
[5] D. A. Wolf-Gladrow, *Lattice-Gas Cellular Automata and lattice Boltzmann Models* (Springer, 2000).
[6] M. E. Kutay, A. H. Aydilek, and E. Masad, Computers and Geotechnics **33**, 381 (2006), ISSN 0266-352X.
[7] S. Ansumali and I. V. Karlin, Phys. Rev. E **66**, 026311 (2002).
[8] S. Ansumali, I. Karlin, C. Frouzakis, and K. Boulouchos, Physica A: Statistical Mechanics and its Applications **359**, 289 (2006), ISSN 0378-4371.
[9] G. H. Tang, W. Q. Tao, and Y. L. He, Phys. Rev. E **72**, 056301 (2005).
[10] Y.-H. Zhang, X.-J. Gu, R. W. Barber, and D. R. Emerson, Phys. Rev. E **74**, 046704 (2006).
[11] S. H. Kim, H. Pitsch, and I. D. Boyd, Phys. Rev. E **77**, 026704 (2008).
[12] S. H. Kim and H. Pitsch, Phys. Rev. E **78**, 016702 (2008).
[13] F. Verhaeghe, L.-S. Luo, and B. Blanpain, J. Comput. Phys. **228**, 147 (2009), ISSN 0021-9991, URL http://portal.acm.org/citation.cfm?id=1460944.1461311.
[14] Z. Guo, C. Zheng, and B. Shi, Phys. Rev. E **77**, 036707 (2008).
[15] Z. Guo and C. Zheng, Int. J. Comput. Fluid Dyn. **22**, 465 (2008), ISSN 1061-8562, URL http://portal.acm.org/citation.cfm?id=1451677.1451682.
[16] F. Toschi and S. Succi, Europhys. Lett. **69**, 549 (2005).
[17] X. B. Nie, X. Shan, and H. Chen, EPL (Europhysics Letters) **81**, 34005 (2008).
[18] L. Mieussens, Journal of Computational Physics **162**, 429 (2000), ISSN 0021-9991.
[19] X. SHAN, X.-F. YUAN, and H. CHEN, Journal of Fluid Mechanics **550**, 413 (2006), http://journals.cambridge.org/article_S0022112005008153, URL http://dx.doi.org/10.1017/S0022112005008153.
[20] H. Grad, Comm. Pure Appl. Math. **2**, 331 (1949).
[21] H. Grad, Comm. Pure Appl. Math. **2**, 325 (1949).
[22] A. Bardow, I. V. Karlin, and A. A. Gusev, Phys. Rev. E **77**, 025701 (2008).
[23] W. Dong, Ph.D. thesis, Univ. California (1956).
[24] P. L. Bhatnagar, E. P. Gross, and M. Krook, Phys. Rev. **94**, 511 (1954).
[25] A. Ghizzo, B. Izrar, P. Bertrand, E. Fijalkow, M. R. Feix, and M. Shoucri, Physics of Fluids **31**, 72 (1988).
[26] C. B. Laney., *Computational gasdynamics* (Cambridge University Press, 1998).
[27] B. Koren, *A Robust Upwind Discretization Method For Advection, Diffusion And Source Terms* (– In: 'Numerical methods for advection-diffusion problems' Pages: 117–138 Series: Notes Numer. Fluid Mech. Vol: 45 – Vieweg (Braunschweig) – 21, 1993).
[28] B. Izrar, A. Ghizzo, P. Bertrand, E. Fijalkow, and M. R. Feix, Computer Physics Communications **52**, 375 (1989), ISSN 0010-4655.